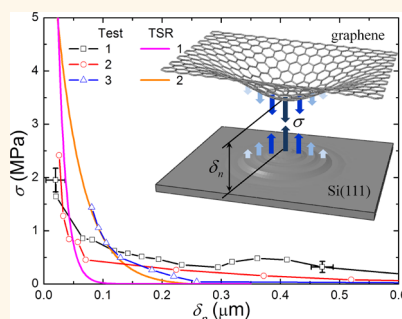


Ultra Long-Range Interactions between Large Area Graphene and Silicon

Seung Ryul Na,^{†,‡} Ji Won Suk,^{§,‡} Rodney S. Ruoff,[‡] Rui Huang,[†] and Kenneth M. Liechti^{*,†}

[†]Department of Aerospace Engineering and Engineering Mechanics Research Center for the Mechanics of Solids, Structures and Materials, [‡]Department of Mechanical Engineering and The Materials Science and Engineering Program, The University of Texas at Austin, Austin, Texas 78712, United States and [§]School of Mechanical Engineering, Sungkyunkwan University, Suwon, 440-746, Republic of Korea. [‡]S.R.N. and J.W.S. contributed equally to this work.

ABSTRACT The wet-transfer of graphene grown by chemical vapor deposition (CVD) has been the standard procedure for transferring graphene to any substrate. However, the nature of the interactions between large area graphene and target substrates is unknown. Here, we report on measurements of the traction–separation relations, which represent the strength and range of adhesive interactions, and the adhesion energy between wet-transferred, CVD grown graphene and the native oxide surface of silicon substrates. These were determined by coupling interferometry measurements of the separation between the graphene and silicon with fracture mechanics concepts and analyses. The measured adhesion energy was $357 \pm 16 \text{ mJ/m}^2$, which is commensurate with van der Waals interactions. However, the deduced traction–separation relation for graphene–silicon interactions exhibited a much longer range interaction than those normally associated with van der Waals forces, suggesting that other mechanisms are present.



KEYWORDS: adhesive interactions · strength · range · energy · graphene · silicon · interferometry

Chemical vapor deposition (CVD) of graphene^{1–3} has greatly expanded its potential applications but requires that it be separated from its metal seed layer. So-called wet transfer,⁴ where the metal layer is etched away, has been the most common approach. Having separated the graphene, the next question to be addressed, particularly when considering scale up to nanomanufacturing processes such as transfer printing or roll-to-roll transfer, is the adhesion of the graphene to target substrates. Such adhesion can be addressed at very fundamental levels, exploring the nature of atomic interactions between graphene and other materials, while having very practical applications in designing, developing and controlling nanomanufacturing processes. It is also related to exploring the potential for dry transfer of graphene from metal seed layers; graphene might be mechanically delaminated from the metal and directly transferred to target substrates. This process has the potential for faster throughput in nanomanufacturing processes and allows the seed metal to be recycled.⁵

Measurement of the adhesion energy of graphene transferred to silicon has been

reported by Zong *et al.*⁶ and Bunch *et al.*^{7,8} who each measured the adhesion energy between exfoliated graphene flakes and thermally grown silicon oxide (280 nm) on Si(100). By draping graphene over nanoparticles deposited on the substrate, Zong *et al.*⁶ obtained the adhesion energy at $151 \pm 28 \text{ mJ/m}^2$. Bunch's group used microblister tests to arrive at values ranging from 450 ± 20^7 to 240 mJ/m^2 .⁸ At larger scales, blister tests have also been used to determine the adhesion energy between CVD grown graphene that had been transferred to copper,⁹ yielding similar levels of adhesion energy. On the other hand, a higher adhesion energy ($720 \pm 70 \text{ mJ/m}^2$) was obtained between as-grown graphene and its seed layer (approximately 300 nm Cu film) by a double cantilever beam fracture test.⁵

The adhesion energy can, by itself, only be used to predict the onset of a delamination at an interface from a pre-existing one using linear elastic fracture mechanics concepts;¹⁰ this simplest approach is a no-go/go indication of crack growth that does not account for the more gradual transition to steady state growth that usually occurs. Prediction of the latter or growth along an interface in the absence of a pre-existing

* Address correspondence to kml@mail.utexas.edu.

Received for review July 3, 2014 and accepted October 15, 2014.

Published online October 15, 2014
10.1021/nn503624f

© 2014 American Chemical Society

delamination requires the strength of the interaction to be known as a function of the separation of the surfaces. This function is known as the traction–separation relation¹¹ and can be viewed as a constitutive entity for the interacting surfaces, separate from the constitutive or stress–strain behavior of each interacting body. The area underneath the traction–separation relation is the adhesion energy.

In situations where the interactions are accessible to atomistic calculations, traction–separation relations can be computed directly from the appropriate classical force fields without resorting to any calibration experiments.¹² They can be viewed as the continuum representation of the interactions between the two surfaces. In more complex cases, the traction–separation relation for a particular contact pair can be determined in a suitable characterization experiment. No matter which route is taken, the traction–separation relation can then be used to predict the onset and growth of contact and/or separation of the pair in some other configuration,¹³ such as transfer printing or roll-to-roll-transfer.

Theoretically, van der Waals (vdW) interactions have been considered as the dominant mechanism for the adhesive interactions between graphene and silicon. Using a semiempirical density functional theory (DFT) approach (DFT-D2) with vdW corrections, Fan *et al.*¹⁴ obtained an adhesion energy of 235 mJ/m² for graphene on a reconstructed crystalline SiO₂ surface. Other DFT calculations with more sophisticated vdW corrections have predicted higher adhesion energy for the same interface (~349 mJ/m²).¹⁵ On the basis of classical force field calculations, the adhesion energy due to vdW interactions between graphene and amorphous silica was found to vary from 149 to 250 mJ/m².¹⁶ In addition to the adhesion energy, the strength and range of vdW interactions have also been predicted, typically with higher strengths (>100 MPa) and shorter ranges (<10 nm) than the traction–separation relations that were measured here.

Although the theoretical predictions of the adhesion energy due to vdW interactions compare closely with our measurements, the traction–separation relations associated with the interactions between graphene and silicon, which are more revealing, have not yet been measured. In this paper, we report on the measurement of the traction–separation relations associated with the interactions between CVD grown graphene and the native oxide layer (2 nm) on Si(111) surfaces. The extent of these measured traction–separation relations was limited by the 20 nm resolution in separation. They were supplemented by continuum analyses with traction–separation relations that matched the measured values beyond separations of 20 nm and considered various strength distributions at smaller separations.

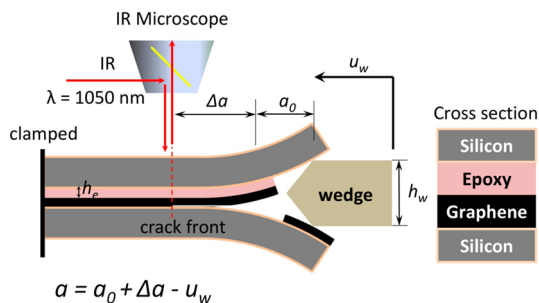


Figure 1. Infrared crack opening interferometry in the fracture experiments.

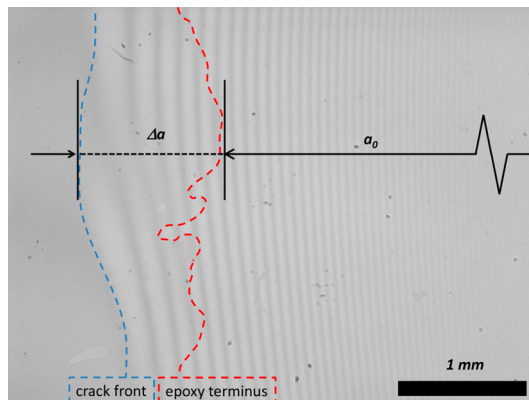


Figure 2. Defining the crack front and crack face separation from fringe patterns. An image of the fringe pattern associated with the crack opening due to the insertion of a wedge in the sandwich specimen. The original epoxy terminus (red dashed line) and the new crack front (blue dashed line) define the crack extension Δa .

RESULTS AND DISCUSSION

CVD grown graphene was transferred to a silicon strip (Figure S1, Supporting Information) and bonded to a second silicon strip with an epoxy that was transparent to infrared. The resulting silicon/graphene/epoxy/silicon laminates (Figure S3) were separated (Figure 1) *via* wedge tests, which are reminiscent of Obreimoff's classic cleavage experiments on mica.¹⁷ Here, the experiments were conducted using a screw-driven wedge that was inserted or withdrawn under displacement control. The crack face separation was measured using infrared crack opening interferometry (IR-COI). Details are given in Supporting Information. The fringes (Figure 2) obtained from infrared crack opening interferometry (IR-COI) indicate that the fracture surfaces were smooth and flat enough to cause interference. This suggests that delamination either occurred along the graphene/silicon, graphene/epoxy or epoxy/silicon interfaces or cohesively within the epoxy layer. Branching between some of these interfaces is also possible. A combination of SEM, AFM and Raman spectroscopy were applied to both fracture surfaces of each specimen in order to determine the fracture path.

The state of the surfaces of bare silicon and graphene coated silicon were examined *via* AFM (Figure S7).

The RMS roughness of the bare silicon (Figure S7a) following piranha treatment was 0.31 nm over $5 \times 5 \mu\text{m}$. Examples of the surface of the graphene following transfer to the silicon exhibit wrinkles and trapped copper residue (Figure S7b) and torn graphene that had curled up (Figure S7d) as well as bubbles, which tend to occur at the junction of wrinkles. The RMS roughness in a number of regions are summarized in Figures S7c,e. The overall RMS roughness of the $5 \times 5 \mu\text{m}$ region in Figure S7c was 5.3 nm. When regions containing copper residues were not included, the RMS roughness ranged from 0.9 to 1.3 nm. For the $5 \times 5 \mu\text{m}$ region in Figure S7e, the overall RMS roughness was 4.9 nm and ranged from 0.5 to 2.1 nm in the boxed regions.

Figure 3a is a schematic side view of a specimen under wedge loading in which it was assumed that the graphene/silicon interface delaminated, initiating near the termination of the epoxy layer above and leaving behind graphene on the lower silicon strip (designated LSi) in the region where there was no epoxy on the upper strip (USi). If this was indeed the case, then the graphene that had been transferred to the lower silicon strip must have been transferred to the epoxy on the upper silicon strip. The corresponding plan view of this scenario is shown in Figure 3b, where the locations examined later in Raman spectroscopy are identified by seven red and four blue spots on USi and LSi, respectively. Relatively low magnification SEM images of the fracture surfaces of the upper and lower strips are shown in Figure 3c. On the left part, the wavy epoxy terminus on USi clearly identifies the boundary between graphene on the epoxy surface and bare silicon. The darker region indicates that there was no charging of the epoxy surface due to the presence of graphene. The gray region corresponds to the bare silicon. The image on the right in Figure 3c is of the surface of LSi, where the boundary between graphene on silicon and bare silicon is apparent but not as clearly as before. In addition, straight line features indicate that the graphene was scratched off the silicon by the wedge in places. This is shown more clearly in AFM scans in Figure S8a. The region enclosed by the orange box in Figure 3c is magnified by $100\times$ in Figure 3d, where the boundary between silicon with and without graphene is clearly visible. Furthermore, the dark lines on the graphene correspond to wrinkles and the hexagonal dark islands may be ad-layers of graphene. The scratched region in the SEM image (Figure 3c) is shown in an AFM scan in Figure S8a. The overall RMS roughness over a $16 \times 14 \mu\text{m}$ region that included the scratches was 2.4 nm. If the scratches were excluded then the RMS roughness was 0.9 nm, and if both scratches and wrinkles were excluded, the RMS roughness dropped to 0.3 nm. Thus, the range of RMS values of graphene on silicon before and after delamination was quite similar.

To confirm that the graphene was indeed removed from the silicon, several spots were interrogated with Raman spectroscopy. Each spot was separated by approximately 1 mm (Figure 3b). The results for the seven spots on the fracture surface of the upper strip (USi) are shown in Figure 3e, where they are compared with the background signal of a pure epoxy layer (the Raman spectra for bare silicon and epoxy appear in Figures S2 and S6, respectively). The seven spots all contained the graphene 2D band at 2700 cm^{-1} , while the G bands of graphene were obscured by the background signal of the epoxy. Raman spectroscopy was also conducted (Figure 3f) on the fracture surface of the lower strip (LSi) at the four spots that were identified in Figure 3b. The striking feature of all these spectra is that there were no signs of the G band or the 2D band. As a result, it can be concluded that graphene was removed from the lower silicon strip and successfully transferred to the epoxy surface on the upper silicon strip.

In previous interfacial fracture experiments between epoxy and silicon,¹⁸ AFM scans of the silicon and epoxy fracture surfaces identified dense ligament formation in regions where the epoxy had preferentially attached to the silicon. Ridge formation has also been observed in previous studies of glass/epoxy interfaces,¹⁹ reflecting a particular mechanism of interfacial crack propagation in these systems. Accordingly, as a control, a wedge test was conducted on a silicon/epoxy/silicon laminate with the IR transparent epoxy that was used in this study. Evidence of ligament formation and ridge formation on the epoxy surface was again evident (Figure 3h), albeit with a much lower density of ligaments.

The AFM scan of the fracture surface of USi is shown in Figure 3g, where it can be seen that there was no ligament or ridge formation at all. This was yet another indication that the graphene had been transferred to the epoxy. The occasional features that did appear on the otherwise smooth graphene surface were bubbles that were as high as 150 nm above the surrounding surface. These bubbles may suggest that the graphene was not completely attached to the epoxy, but further study of this phenomenon is required. The overall RMS roughness over a $7 \times 10 \mu\text{m}$ region removed from the large bubbles was 9.7 nm. Smooth regions away from bubbles had RMS roughness values ranging from 0.4 to 0.7 nm.

Figure 4 shows a typical set of responses to the insertion of the wedge in three different samples. Each of the crack lengths noted in the figure was measured at the end of the 30-s interval for a given wedge position. It can be seen that the responses were originally linear as the wedge was inserted without any crack growth. The responses became nonlinear as the crack started to grow and soon achieved steady state in the sense that the crack length remained the same following each wedge insertion.

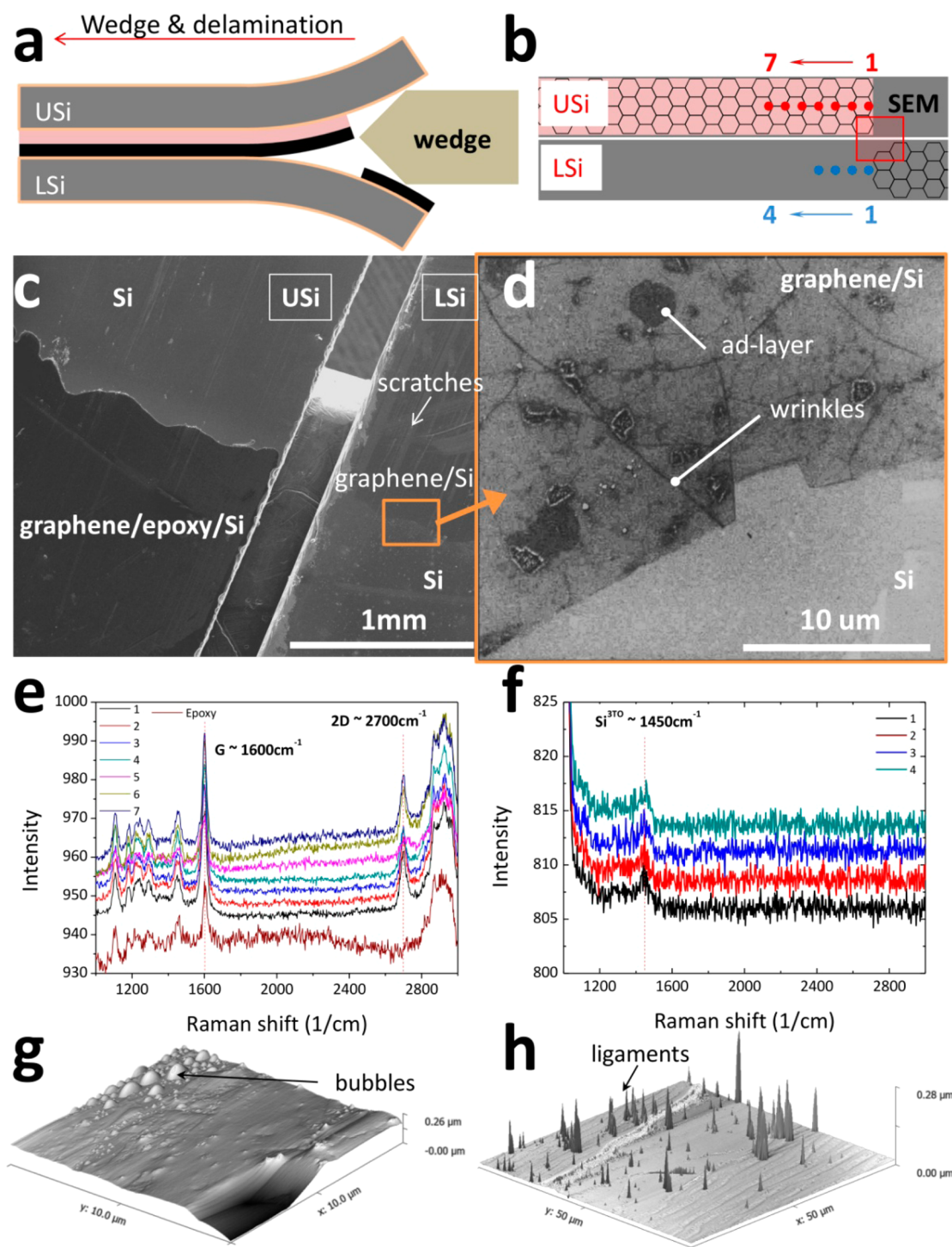


Figure 3. Characterization of the fracture surfaces. (a) Edge view schematic of graphene delamination from the lower silicon strip. (b) Plan view schematic of the fracture surfaces of both silicon strips after complete separation. (c) Low magnification SEM image of the fracture surfaces of both silicon strips and (d) high magnification SEM image of the fracture surface of the lower silicon strip. (e) Raman spectra of the fracture surface of the upper silicon strip at 7 different spots. (f) Raman spectra of the fracture surface of the lower silicon strip at 4 different spots. (g) Microbubbles between graphene and epoxy on a $10\ \mu\text{m}$ by $10\ \mu\text{m}$ AFM scan of the fracture surface of the upper silicon strip. (h) Epoxy ligaments on a $50\ \mu\text{m}$ by $50\ \mu\text{m}$ AFM scan of the epoxy fracture surface of a silicon/epoxy/silicon specimen with no graphene.

A typical set of NCOD profiles measured by IR-COI for the third specimen is shown in Figure 5. A number of such profiles are shown as the wedge was inserted in order to capture the initial opening of the crack faces

without growth, through initiation and subsequent steady state growth.

Using intensity measurements provided very precise measurements of the crack extension, Δa . As a result, it

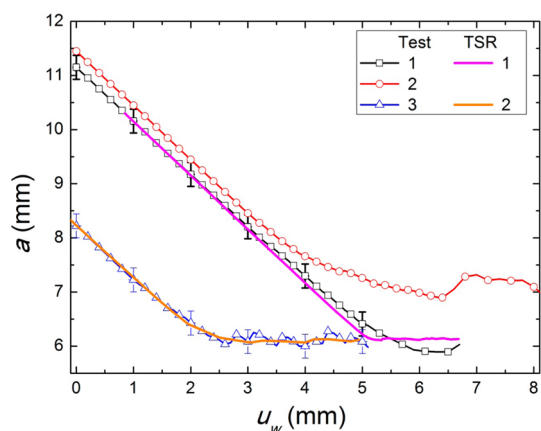


Figure 4. Variation of crack length with respect to wedge insertion. The initially linear response indicates that the crack was not growing as the wedge was inserted. Subsequent crack extension soon transitioned to steady state growth where each wedge insertion step produced the same amount of growth. Finite element solutions are shown as TSR1 and TSR2 as simulations of both tests 1 and 2 and test 3, respectively.

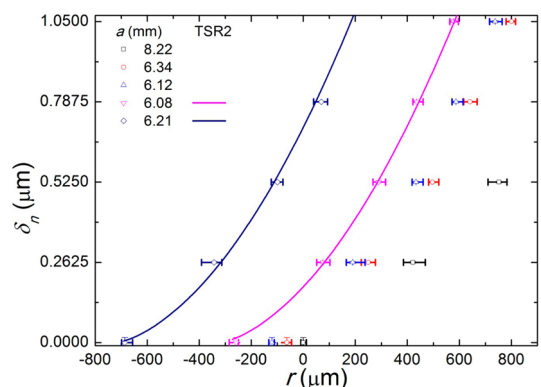


Figure 5. Crack face separation during crack opening and growth. NCOD profiles obtained by IR-COI as a function of crack length a as the wedge insertion progressed during test 3. Finite element solutions are shown as TSR2 for two steady state growth conditions.

was possible to obtain high fidelity delamination resistance curves (Figure 6) associated with the silicon/graphene interactions. The results from the three different specimens (test 1 and 2 in Figure 6a and test 3 in Figure 6b) were quite consistent although specimen 3 exhibited a steeper increase in delamination resistance prior to some “stick–slip” behavior, which suggests that the adhesion between graphene and silicon may have been slightly different in this case. For example, the presence of trapped copper residue, and number cracks and wrinkles (Figure S7b,d) in the graphene may differ from sample to sample and manifest in the slight differences noted here. Nonetheless, the results from Raman spectroscopy did indicate that the graphene was a monolayer. In all cases, the J-integral (eq 1 in Methods) grew steeply from zero to between 100 to 180 mJ/m^2 for small amounts of growth ($<3 \mu\text{m}$), below the uncertainty in measurements of crack extension.²⁰ The rate of

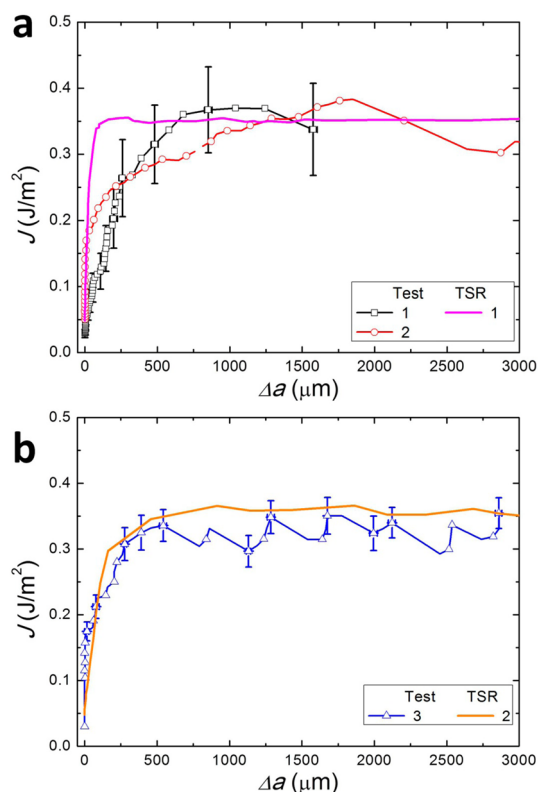


Figure 6. Delamination resistance behavior for graphene/silicon interactions. The resistance to fracture as represented by the J-integral initially rose steeply with small amounts of crack extension Δa . The resistance to crack growth eventually stabilized at the steady state toughness Γ_{ss} of the graphene/silicon interface. (a) A comparison of the resistance response with respect to data from tests 1 and 2 and a finite element solution using TSR 1. (b) A comparison of the resistance response with respect to data from test 3 with a finite element solution using TSR 2.

increase in the J-integral decreased with increasing crack extension and eventually reached a plateau after crack extensions of 0.7 to 2 mm. The J-integral at the plateau was considered to be the steady state toughness Γ_{ss} at $357 \pm 16 \text{ mJ}/\text{m}^2$, which was the average and standard deviation of all peak values once the plateau had been achieved in each specimen. This value is about $90 \text{ mJ}/\text{m}^2$ lower than previous results reported by Koenig *et al.*,⁷ but $120 \text{ mJ}/\text{m}^2$ higher than the value reported in the literature.⁸ It is not clear at this time whether or not this is a significant difference. However, in both reports,^{7,8} the graphene was exfoliated from graphite and the silicon oxide layer was approximately 300 nm thick grown on a Si(100) surface. In this study, the CVD grown graphene was wet-transferred from its copper seed layer to the Si(111) with an approximately 2 nm-thick native oxide layer with a root mean squared (RMS) roughness less than 0.5 nm (Figure S7a). In addition, there may also have been differences in the nature of any liquid trapped between the graphene and silicon in each case when the graphene was wet-transferred to silicon substrate.

In addition, the traction–separation relation associated with silicon/graphene interactions can be obtained

by measuring the development of the J-integral with respect to δ_n^* . Such data is shown (Figure 7a) for the same three samples. Similar to the resistance curves in Figure 6, there was a very steep rise in the value of the J-integral before the NCOD exceeded the resolution of the IR-COI. Subsequently, the J-integral increased gradually before reaching steady state.

The corresponding traction–separation relation (Figure 7b) was determined by applying eq 3 (see Methods) to the data in Figure 7a using a central difference scheme. In each case, the traction–separation relations obtained in this way had very steep increases to the maximum value of the traction that could be measured given the resolution in NCOD. Note that this was not necessarily the actual maximum strength σ_0 of the interaction at the associated separation δ_n^0 (insert to Figure 7b). The tractions then decayed to zero at δ_n^c , the critical separation for fracture. The area under the traction–separation relation equals the steady state toughness Γ_{ss} (adhesion energy), while the strength and range of the interactions are characterized by the maximum strength (σ_0) and the critical separation (δ_n^c), respectively. The values of these parameters for each experiment are recorded in Table 1. The critical NCOD were the most difficult parameters to assign values to because of the long tails of the distributions and the levels of uncertainty in the measurements.

Looking at Figure 7b, it can be seen that the measured traction–separation relations obtained from the first two samples were quite similar. The initial stiffness, measured strength and the critical NCOD from the third sample were all noticeably lower. From Table 1, the measured strengths for samples 1 and 2 were between 1.95 and 2.42 MPa at associated NCOD δ_n^0 of 19.84 and 25.9 nm. The values of δ_n^c were estimated to be 820 and 530 nm, respectively for specimens 1 and 2. While the value of the adhesion energy (366 and 377 mJ/m^2) compares closely with predictions for vdW interactions,¹⁵ the range of the interactions are much longer than vdW. Hence, the present results challenge the current understanding that vdW interactions are the dominant mechanism for the adhesive interactions between graphene and silicon. The interaction ranges for electrostatic interactions between graphene and silicon are in the nanometer range²¹ thereby ruling them out as a potential mechanism for the interactions measured here. A likely mechanism for the observed long-range interactions may be capillary effects, although the interaction range for capillary forces due to water menisci is typically less than 5 nm^{22,23} on smooth surfaces. One factor that might explain the noted differences is the roughness of the silicon substrate and how well graphene can conform. The combined effects of surface roughness and capillary forces could in principle extend the interactions to longer ranges but reduce the magnitude of tractions. The RMS roughness of the Si(111) surface considered in this

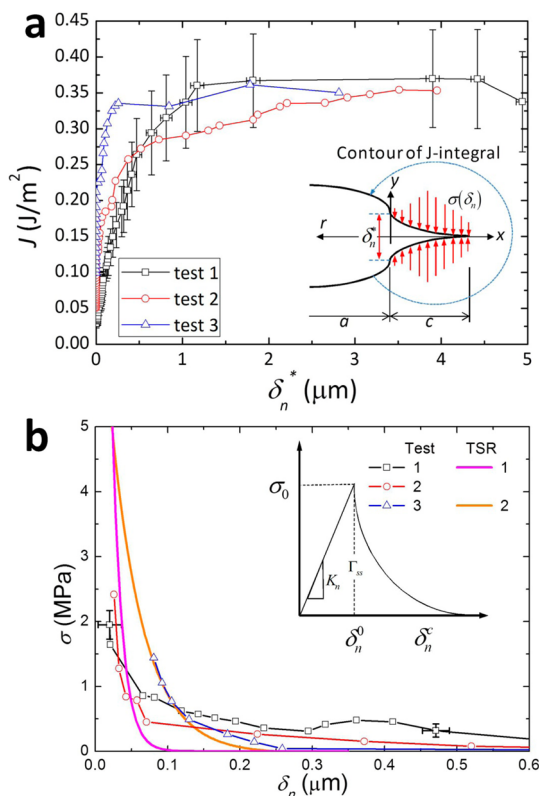


Figure 7. Essence of determining traction–separation relations for graphene/silicon interactions. (a) The variation of the J-integral with respect to the normal crack tip opening displacement δ_n^* is determined (the inset defines the cohesive zone geometry and interactions). (b) The derivative of this data yields the corresponding traction–separation relation (the inset identifies the parameters listed in Table 1). TSR1 and TSR2 are the traction–separation relations that were used in the finite element analyses of tests 1 and 2 and test 3, respectively.

TABLE 1. Summary of Parameters Associated with the Measured Traction–Separation Relations for Each Different Experiment

	test 1	test 2	test 3	average
σ_0^a (MPa)	1.951	2.415	1.4	1.922 \pm 0.414
δ_n^0 (nm)	19.84	25.9	81.01	42.25 \pm 33.7
δ_n^c (nm)	820	530	300	550 \pm 260
Γ_{ss} (mJ/m^2)	366 \pm 4	377 \pm 5	343 \pm 8	357 \pm 16

^a Note that the values of σ_0 listed here were the maximum strengths that could be measured and were not necessarily the maximum strength of the interaction due to the 20 nm resolution limit in the measured separations.

study is less than 0.5 nm (Figure S7a), which is much less than the range of RMS roughness (2.6 to 10.3 nm) that was considered by DelRio *et al.*²⁴ for vdW interactions between polysilicon surfaces. Capillary effects were also considered^{25,26} over the same range of roughness. In both cases, the roughness effect brought the interaction range into registration with the values measured here. However, the adhesion energies were much lower ($\sim \mu\text{J/m}^2$) and no information on traction levels was provided.

TABLE 2. Summary of Parameters Associated with the Traction–Separation Relations for Finite Element Simulations

	TSR1	TSR2
σ_0 (MPa)	24	8
δ_n^0 (nm)	2	2
δ_n^c (nm)	150	250
α	25	5.5
Γ_{ss} (mJ/m ²)	358	360

In order to provide more insight into the strength of the interactions at separations below the resolution of the IR-COI a parametric study of potential traction–separation relations was conducted using finite element analysis (see Methods). Two traction–separation relations (Table 2) were considered in the analysis. One (TSR1) matched the measured traction–separation relations from tests 1 and 2 while TSR2 corresponded to the traction–separation relation from test 3. While these traction–separation relations matched the measurements in the range where they could be measured (Figure 7b), they both continued the interactions closer to zero separation. The maximum strength for TSR1 was 24 MPa at 2 nm with $\alpha = 25$ and a cutoff separation of 150 nm for an adhesion energy of 357 mJ/m². The corresponding parameters for TSR2 were 8 MPa, 2, 5.5, 250 nm and 360 mJ/m². TSR1, which was constrained by eq 4, matched the measured traction–separation relations quite well from 20 to 70 nm but did not capture the long tail. The fit between TSR2 and the data from test 3 was excellent over the entire range of measurements. The finite element solutions for the variation of crack length with respect to wedge insertion (Figure 4), crack opening displacements (Figure 5) and resistance curves (Figure 6) were all compared with measurements.

In Figure 4, it can be seen that the solution with TSR1 was in good agreement with the data from test 1, but not test 2. This was because the adhesion energy of 357 mJ/m², which was selected for TRS1 as the average of all steady state adhesion values, was close to the adhesion energy that was measured in test 1. The agreement between the solution for TSR2 and the data from test 3 was excellent. It should also be noted that the transition from no growth to steady state growth is more gradual when the range of the interactions is longer. The NCOD shown in Figure 5 were measured in test 3. The finite element solutions using obtained TSR2 for steady state growth are compared with data when the crack was 6.08 and 6.21 mm long. It can be seen that the agreement was quite good. The solution for the resistance curve with TSR1 (Figure 6a) initially rose more steeply than the data but reached the steady state adhesion that was measured in test 1 for the reasons given earlier. The reason for the steeper rise

was that TRS1 did not capture the more gradual decay of the measured traction–separation relations from tests 1 and 2. This point is brought out very well in Figure 6b, where the solution for TSR2 had a similar rise as the data and reached the adhesion of 360 mJ/m², which corresponded to the peaks of the measured stick–slip behavior.

If a vdW interaction with a maximum strength of 200 MPa and critical separation of 3 nm had been used as a traction–separation relation in the finite element analysis, it is clear that it would not match any of the measured portions of the traction–separation relations. Furthermore, the transition from no growth to steady state growth (Figure 4) would have been very abrupt (Figure S9). Capillary interactions have been represented by a constant strength at 35 MPa for 5 nm with an adhesion energy of 175 mJ/m². While such an interaction would still provide a sharp transition from no growth to steady state growth for the reason given above, the lower adhesion energy of capillary effects would cause the crack to grow at much longer crack lengths. The effect of either interaction on the NCOD would not be visible at the scales shown in Figure 5. The effect of longer interaction ranges is also apparent in the resistance curves (Figure 6 and S9). For example, the longer interaction range of TSR2 resulted in a more gradual rise in the J-integral prior to steady state growth. If a longer interaction range could have been incorporated in TSR1, it would have matched the more gradual rise in the J-integral prior to steady state growth that is apparent in the data. These observations support the claim that neither van der Waals nor capillary interactions were at play here.

The roughness of the graphene on silicon ranged from 0.4 to 5 nm due to defects such as wrinkles, trapped copper residues and torn graphene. This affected the shape of the rising portion of the resistance curves (Figure 6), the steady state toughness and the traction–separation relations. As a result, the long-range interactions that have been observed in this study are most likely reflections of the effect of roughness, which sets the stage for future investigations.

CONCLUSIONS

A fracture mechanics approach was developed to determine the adhesion energy and traction–separation relations associated with the interactions between CVD grown graphene and silicon to which the graphene had been transferred using a wet transfer process. By bonding a second strip to the graphene surface with an epoxy and then peeling the silicon strips apart in a wedge test, interfacial crack growth between graphene and silicon was observed and analyzed. The crack length and NCOD were measured as a function of wedge insertion using IR-COI. This data was then coupled with fracture mechanics analyses to extract the adhesion energy, delamination resistance behavior

and traction–separation relations associated with interactions between graphene and silicon.

The adhesion energy of $357 \pm 16 \text{ mJ/m}^2$ obtained in the present study was bounded by previously reported values for exfoliated graphene flakes, suggesting that the process of wet transferring polycrystalline CVD grown graphene on Si(111) over relatively large areas has no adverse effects. Furthermore, it was in reasonable agreement with theoretical predictions for vdW forces between graphene and silicon, but probably for the wrong reasons. The range of interactions was beyond those usually attributed to retarded vdW interactions. The maximum strength that could be measured was most likely lower than the actual one

because the resolution in the measurement of separation was not sufficient to capture it. This was brought out in subsequent continuum analyses with traction–separation relations which captured the measured interactions and extended them to smaller separations and higher tractions. The combinations of experiments and analysis described here should provide a basis for subsequent models of the nature of graphene/silicon over relatively large spatial dimensions. Such developments will have to account for the effects roughness and humidity on long-range interactions. The approach developed here can be extended to other two-dimensional materials and substrates.

METHODS

Details are provided of the experimental procedures and analysis that were used to obtain the results just presented.

Experiment. Following CVD growth of graphene on copper foils,¹ monolayer graphene was wet-transferred from the seed copper foil to silicon strips (Figure S1).^{4,27,28} Its presence was verified by the existence of G and 2D bands in the Raman spectra (Figure S2). A second silicon strip was bonded to the free surface of the graphene using an epoxy that was transparent to infrared. The resulting silicon/graphene/epoxy/silicon laminates (Figure S3) were separated *via* wedge tests, which are reminiscent of Obreimoff's classic cleavage experiments on mica.¹⁷ Here, the experiments were conducted using a screw-driven wedge that was inserted or withdrawn under displacement control as shown schematically in Figure 1. The left end of the specimen was clamped in order to provide a vertical reference state for easier focusing of the IR microscope and to react the axial load applied by the wedge. The thickness of the silicon strips and epoxy were h and h_e , respectively. The wedge, with a thickness h_w was inserted from the right end by a displacement u_w , which was applied in 0.1 mm loading steps using a micrometer drive. The initial crack length a_0 was measured from the epoxy terminus to the shoulder of the wedge. Subsequent crack extension Δa due to wedge insertion was measured from the IR fringe patterns (Figure 2). At any particular time, the measured crack length was obtained from $a = a_0 + \Delta a - u_w$.

The initial crack in Figure 2 was produced by the limited spreading ($\sim 75\%$) of the epoxy along the silicon strip, resulting in essentially blunt cracks with sometimes irregular fronts (red dashed line) at the termination of the epoxy. As a result, it was necessary to insert the wedge until a small amount of growth, Δa , occurred (Figure 2). It was then withdrawn, leaving a sharp crack with a more regular crack front (blue dashed line), which was taken to be the redefined initial crack length a_0 .

To begin an experiment, the wedge was reinserted with 0.1 mm steps being applied in 10 s followed by a hold time of 20 s. During this 30-s period, interference data near the crack front were recorded every second using the time-lapse feature of the IR camera. Intensity profiles along a line perpendicular to the crack front were extracted from the interference fringes using image processing software. This data was then used to determine the separation of the crack faces (eqs S4–S7) in the Supporting Information, commonly referred to as the normal crack opening displacements (NCOD). The extracted NCOD profiles and crack front locations were then synchronized with the wedge insertion data. Following each wedge test, the fracture surfaces were carefully analyzed *via* SEM, AFM and Raman spectroscopy. This allowed the fracture path to be associated with the measured adhesion energy and traction–separation relations for the delaminated interface.

Analysis. To evaluate the adhesion energy or the fracture toughness of the graphene/silicon interface, we calculated the

J-integral, which is a measure of the energy available for separation. On the basis of simple elastic beam theory, the J-integral under wedge loading is

$$J = \frac{3E_{\text{Si}}h^3(h_w - h_e)^2}{16a^4} \quad (1)$$

where E_{Si} is the in-plane Young's modulus (169 GPa) for Si(111). In the experiments that were conducted here, the crack lengths were such that $a \gg 20h$, which is sufficient for simple beam theory and transverse shear effects could be neglected.²⁹

Thus, by measuring the crack length at any particular wedge insertion, eq 1 allows the J-integral to be determined as a function of crack extension in order to obtain the delamination resistance curve for the silicon/graphene interface. Furthermore, from the NCOD measurements, the J-integral can also be tracked as a function of the normal crack tip opening displacement, δ_n^* , which is the NCOD at the initial crack front (see inset to Figure 7a). Such data can be used to extract the traction–separation relation for a particular interface.^{29,20,30–32}

To summarize the approach, we make use of the fact that the J-integral can also be determined from a local contour surrounding the cohesive zone (Figure 7a insert),

$$J = \int_0^{\delta_n^*} \sigma(\delta_n) d\delta_n \quad (2)$$

where σ is the normal traction acting on the crack faces within the cohesive zone and $\sigma(\delta_n)$ is the normal traction–separation relation that is to be determined. Taking the derivative of eq 2 with respect to δ_n^* leads to

$$\sigma(\delta_n) = \frac{dJ}{d\delta_n^*} \quad (3)$$

Since the J-integral is path independent, its value can be obtained from eq 1 and tracked as a function of δ_n^* , thereby allowing the derivative in eq 3 to be taken in order to extract the corresponding traction–separation relation.

In order to provide some insight into the portion of the traction–separation relations that could not be measured by the procedure just described due to the 20 nm-resolution in crack face separation, a series of finite element analyses were conducted using the commercial code ABAQUS. The linearly elastic behavior of the silicon was accounted using the in-plane Young's modulus for Si(111) given above and a Poisson's ratio of 0.2. The linearly elastic behavior of the epoxy was initially accounted for with a modulus of 3 GPa and a Poisson's ratio 0.4. However, the computation times were extremely long and convergence was often difficult, and resulting separations were within 5.6% difference of calculations that ignored the presence of the epoxy. The results that are presented here were obtained from solutions that neglected the epoxy layer. The analyses also accounted for interactions between the graphene and silicon

through traction–separation relations (insert Figure 7b) that had the form

$$\sigma = K_n \delta_n H(\delta_n^0 - \delta_n) + \sigma_0 \left(1 - \frac{1}{1 - e^{-\alpha}} \right) + \frac{\sigma_0}{1 - e^{-\alpha}} e^{-\alpha \left(\frac{\delta_n}{\delta_n^0} - \frac{\delta_n^0}{\delta_n^0} \right)} H(\delta_n - \delta_n^0) \quad (4)$$

where δ_n is the separation of the crack surfaces at any location, K_n governs the elastic portion of the interaction, the parameter α governs the decay of the interaction and H is the Heaviside step function. This form is the so-called exponential decay traction–separation relation, which was the best of two options available in ABAQUS.

Conflict of Interest: The authors declare no competing financial interest.

Acknowledgment. The authors gratefully acknowledge partial financial support of this work by the National Science Foundation through Grant No. CMMI-1130261. This work is also based upon work supported in part by the National Science Foundation under Cooperative Agreement No. EEC-1160494. Any opinions, findings and conclusions or recommendations expressed in this material are those of the author(s) and do not necessarily reflect the views of the National Science Foundation. One author (J.W.S.) acknowledges the support of the Basic Science Research Program through the National Research Foundation of Korea (NRF) funded by the Ministry of Science, ICT & Future Planning (NRF-2014R1A1A1004818).

Supporting Information Available: The following information is available for interested readers: preparation of silicon strips, wet transfer, verification of graphene transfer, fabrication of fracture specimens, infrared crack opening interferometry (IR-COI), epoxy layer transparency and Raman characteristics, AFM scanning on bare silicon and graphene-coated silicon, graphene scratches, effect of interaction range on delamination resistance curves. This material is available free of charge via the Internet at <http://pubs.acs.org>.

REFERENCES AND NOTES

- Li, X.; Cai, W.; An, J.; Kim, S.; Nah, J.; Yang, D.; Piner, R.; Velamakanni, A.; Jung, I.; Tutuc, E. Large-Area Synthesis of High-Quality and Uniform Graphene Films on Copper Foils. *Science* **2009**, *324*, 1312–1314.
- Tao, L.; Lee, J.; Chou, H.; Holt, M.; Ruoff, R. S.; Akinwande, D. Synthesis of High Quality Monolayer Graphene at Reduced Temperature on Hydrogen-Enriched Evaporated Copper (111) Films. *ACS Nano* **2012**, *6*, 2319–2325.
- Batzill, M. The Surface Science of Graphene: Metal Interfaces, CVD Synthesis, Nanoribbons, Chemical Modifications, and Defects. *Surf. Sci. Rep.* **2012**, *67*, 83–115.
- Li, X.; Zhu, Y.; Cai, W.; Borysiak, M.; Han, B.; Chen, D.; Piner, R. D.; Colombo, L.; Ruoff, R. S. Transfer of Large-Area Graphene Films for High-Performance Transparent Conductive Electrodes. *Nano Lett.* **2009**, *9*, 4359–4363.
- Yoon, T.; Shin, W. C.; Kim, T. Y.; Mun, J. H.; Kim, T.-S.; Cho, B. J. Direct Measurement of Adhesion Energy of Monolayer Graphene as-Grown on Copper and Its Application to Renewable Transfer Process. *Nano Lett.* **2012**, *12*, 1448–1452.
- Zong, Z.; Chen, C.-L.; Dokmeci, M. R.; Wan, K.-T. Direct Measurement of Graphene Adhesion on Silicon Surface by Intercalation of Nanoparticles. *J. Appl. Phys.* **2010**, *107*, 026104.
- Koenig, S. P.; Boddeti, N. G.; Dunn, M. L.; Bunch, J. S. Ultrastrong Adhesion of Graphene Membranes. *Nat. Nanotechnol.* **2011**, *6*, 543–546.
- Boddeti, N. G.; Koenig, S. P.; Long, R.; Xiao, J.; Bunch, J. S.; Dunn, M. L. Mechanics of Adhered, Pressurized Graphene Blisters. **2013**; arXiv preprint arXiv:1304.1011.
- Cao, Z.; Wang, P.; Gao, W.; Tao, L.; Suk, J.; Ruoff, R.; Akinwande, D.; Huang, R.; Liechti, K. A Blister Test for Interfacial Adhesion of Large-Scale Transferred Graphene. *Carbon* **2014**, *69*, 390–400.
- Kanninen, M. F.; Popelar, C. L. *Advanced Fracture Mechanics*; Oxford University Press: Oxford, U.K., 1985.
- Needleman, A. An Analysis of Tensile Decohesion Along an Interface. *J. Mech. Phys. Solids* **1990**, *38*, 289–324.
- Cole, D. J.; Payne, M. C.; Csányi, G.; Spearing, S. M.; Ciacchi, L. C. Development of a Classical Force Field for the Oxidized Si Surface: Application to Hydrophilic Wafer Bonding. *J. Chem. Phys.* **2007**, *127*, 204704.
- Mohammed, I.; Liechti, K. M. Cohesive Zone Modeling of Crack Nucleation at Bimaterial Corners. *J. Mech. Phys. Solids* **2000**, *48*, 735–764.
- Fan, X.; Zheng, W.; Chihai, V.; Shen, Z.; Kuo, J.-L. Interaction between Graphene and the Surface of SiO₂. *J. Phys.: Condens. Matter* **2012**, *24*, 305004.
- Gao, W.; Xiao, P.; Henkelman, G.; Liechti, K. M.; Huang, R. Interfacial Adhesion between Graphene and Silicon Dioxide by Density Functional Theory with Van Der Waals Corrections. *J. Phys. D: Appl. Phys.* **2014**, *47*, 255301.
- Paek, E.; Hwang, G. S. A Computational Analysis of Graphene Adhesion on Amorphous Silica. *J. Appl. Phys.* **2013**, *113*, 164901.
- Obreimoff, J. The Splitting Strength of Mica. *Proc. R. Soc. London, Ser. A* **1930**, *127*, 290–297.
- Gowrishankar, S. *Characterization of Delamination in Silicon/Epoxy Systems*; University of Texas: Austin, TX, 2014.
- Swadener, J.; Liechti, K. Asymmetric Shielding Mechanisms in the Mixed-Mode Fracture of a Glass/Epoxy Interface. *J. Appl. Mech.* **1998**, *65*, 25–29.
- Liechti, K. M.; Na, S. R.; Wakamatsu, M.; Seitz, O.; Chabal, Y. A High Vacuum Fracture Facility for Molecular Interactions. *Exp. Mech.* **2013**, *53*, 231–241.
- Sabio, J.; Seoanez, C.; Fratini, S.; Guinea, F.; Neto, A. C.; Sols, F. Electrostatic Interactions between Graphene Layers and Their Environment. *Phys. Rev. B* **2008**, *77*, 195409.
- Pallares, G.; Grimaldi, A.; George, M.; Ponsion, L.; Ciccotti, M. Quantitative Analysis of Crack Closure Driven by Laplace Pressure in Silica Glass. *J. Am. Ceram. Soc.* **2011**, *94*, 2613–2618.
- Maugis, D.; Gauthier-Manuel, B. JKR-DMT Transition in the Presence of a Liquid Meniscus. *J. Adhes. Sci. Technol.* **1994**, *8*, 1311–1322.
- DelRio, F. W.; de Boer, M. P.; Knapp, J. A.; Reedy, E. D.; Clews, P. J.; Dunn, M. L. The Role of Van Der Waals Forces in Adhesion of Micromachined Surfaces. *Nat. Mater.* **2005**, *4*, 629–634.
- DelRio, F. W.; Dunn, M. L.; Phinney, L. M.; Bourdon, C. J.; de Boer, M. P. Rough Surface Adhesion in the Presence of Capillary Condensation. *Appl. Phys. Lett.* **2007**, *90*, 163104.
- DelRio, F. W.; Dunn, M. L.; de Boer, M. P. Capillary Adhesion Model for Contacting Micromachined Surfaces. *Scri. Mater.* **2008**, *59*, 916–920.
- Suk, J. W.; Kitt, A.; Magnuson, C. W.; Hao, Y.; Ahmed, S.; An, J.; Swan, A. K.; Goldberg, B. B.; Ruoff, R. S. Transfer of CVD-Grown Monolayer Graphene onto Arbitrary Substrates. *ACS Nano* **2011**, *5*, 6916–6924.
- Suk, J. W.; Lee, W. H.; Lee, J.; Chou, H.; Piner, R. D.; Hao, Y.; Akinwande, D.; Ruoff, R. S. Enhancement of the Electrical Properties of Graphene Grown by Chemical Vapor Deposition via Controlling the Effects of Polymer Residue. *Nano Lett.* **2013**, *13*, 1462–1467.
- Gowrishankar, S.; Mei, H.; Liechti, K. M.; Huang, R. A Comparison of Direct and Iterative Methods for Determining Traction–Separation Relations. *Int. J. Fract.* **2012**, *177*, 109–128.
- Sørensen, B. F.; Jacobsen, T. K. Determination of Cohesive Laws by the J-Integral Approach. *Eng. Fract. Mech.* **2003**, *70*, 1841–1858.
- Sørensen, B. F.; Kirkegaard, P. Determination of Mixed Mode Cohesive Laws. *Eng. Fract. Mech.* **2006**, *73*, 2642–2661.
- Zhu, Y.; Liechti, K. M.; Ravi-Chandar, K. Direct Extraction of Rate-Dependent Traction–Separation Laws for Polyurea/Steel Interfaces. *Int. J. Solids Struct.* **2009**, *46*, 31–51.